NASA-CR-200738

CAL-2450

National Aeronautics and Space Administration

EUVE GUEST INVESTIGATOR PROGRAM

ANNUAL STATUS REPORT FOR NAG 5-2569

Submitted by:

The Trustees of Columbia University
in the City of New York
351 Engineering Terrace
New York, New York 10027

Prepared by:

Columbia Astrophysics Laboratory
Departments of Astronomy and Physics
Columbia University
538 West 120^{th} Street
New York, New York 10027

Principal Investigator:

Jules P. Halpern
Associate Professor of Astronomy

Title of Research: **"The Nearest Neutron Stars" funded as a suppl. to "Distance to the Geminga Pulsar"**

Period Covered by Report: 15 April 1994 – 14 April 1996

April 1996

TABLE OF CONTENTS

1. EUVE Observation of the Binary Millisecond Pulsar PSR J0437–4715

The 5.75 ms pulsar J0437–4715, discovered by Johnston et al. (1993), is the nearest millisecond pulsar at $d = 140$ pc, and is also in a 5.74 d binary orbit with a cool white dwarf companion of mass $\sim 0.2 M_\odot$ Its radio emission is so bright that individual pulses are easily seen. It is also the only millisecond pulsar from from which pulsed X-rays have been detected and one of two surrounded by a bow-shock nebula. Fundamental questions about PSR J0437–4715 and other millisecond pulsars are 1) whether or not its characteristic age, $P/2\dot{P}$, is consistent with the cooling age of its white dwarf companion, 2) whether its X-rays are magnetospheric in origin or thermally reheated surface emission, and 3) why it is not (yet) a detectable high-energy γ-ray source.

The nature of the soft X-ray emission from PSR J0437–4715 is still not clear. In addition to the mostly power-law spectrum, a blackbody component of temperature $T \sim 1.7 \times 10^6$ K and emitting area 0.05 km^2 might be be present that is associated with a peak at 0.9 keV in the pulsed fraction as a function of energy. Such a component would, of course, demand the operation of some mechanism of surface reheating; in all calculations neutron stars cool below 10^5 K after 10^6 yr.

A previous, shorter *EUVE* observation of PSR J0437–4715 was reported by Edelstein, Foster, & Bowyer (1995), but those data were not taken in the high time resolution mode which is necessary to see the pulsations. Furthermore, combined analysis of the *EUVE* and *ROSAT* pulse profiles and spectra enable us to reassess the question of thermal vs. nonthermal X-ray emission, and to place formal limits on the properties of any thermal components that may be present.

The pulsar J0437–4715 was observed by *EUVE* during a 20 day period between 1994 October 23 and November 12, during which a valid exposure time of 495,897 s was obtained in the Deep Survey (DS) instrument. Events occurring when the line of sight to the source passed less than 450 km above the Earth's limb were rejected. A total of 4370 counts above background were collected from the pulsar through the Lexan filter, as determined in a 73″ radius extraction aperture. After accounting for deadtime and "Primbsching" (losses due to telemetry sharing between instruments), the effective exposure time is reduced to 449,034 s. The resulting corrected count rate of 0.00973 ± 0.00017 s^{-1} was used in all calculations that require an absolute flux. To maximize the signal-to-noise ratio in the pulsed light curve, we also extracted counts within a smaller aperture of the DS, a carefully placed circle of radius 43″ which contains 95% of the source counts in the asymmetric source profile. The resulting light curve contains an estimated 4163 source counts, and only 937 background events. (Data were taken simultaneously by the three spectrometers pointed at the source, but no significant detection of the pulsar was made in these. The spectrometer data will not be discussed further here.)

We first transformed the time of arrival of each photon to Barycentric Dynamical Time (TDB) using a procedure based on the Princeton TEMPO code, supplemented with the additional corrections for the changing orbital position of the *EUVE* satellite. The photon times were then corrected for the orbital Doppler delay within the 5.74 d binary system. The resulting pulse profile is shown in Figure 1. Background has been subtracted, and two cycles are graphed to guide the eye. There is one broad pulse per cycle, although it is narrower than a sinusoid. The pulsed fraction, defined conventionally as the fraction of the

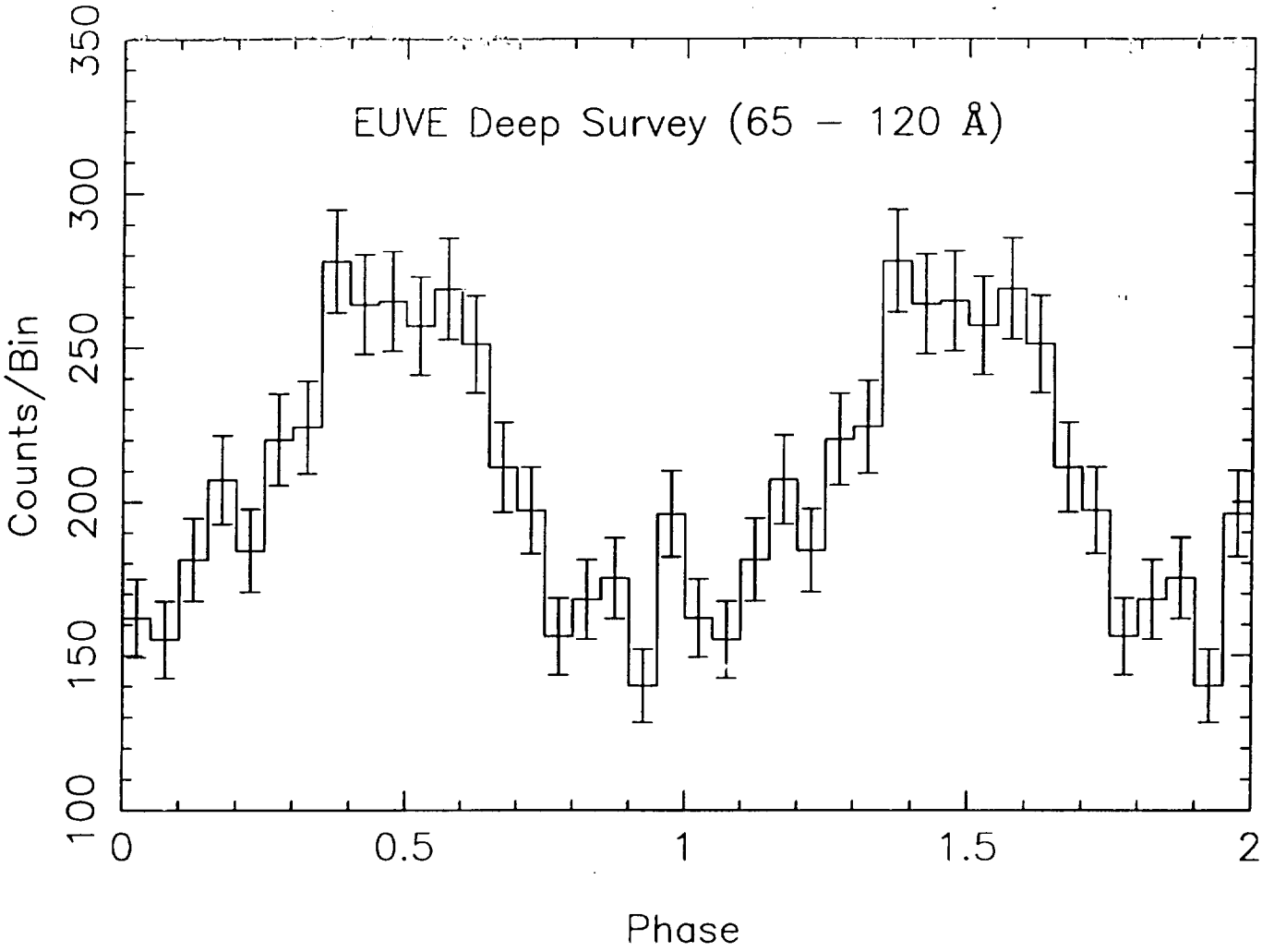

FIG. 1. - Pulse profile of the 5.75 ms pulsar J0437–4715 from the *EUVE* Deep Survey instrument. Background has been subtracted. The phase is arbitrary. Note that the time resolution is at best 0.5 ms, or 2 bins in the light curve. The data are repeated for two cycles to guide the eye. The pulsed fraction is 0.27 ± 0.05.

total counts lying above the minimum of the light curve, is 0.27 ± 0.05. The peak-to-trough ratio is approximately 1.8.

It is important to understand the possible sources of systematic error in the pulse profile in terms of the various effects that limit the accuracy of the final timing solution. A measurement of the pulse shape of this 5.75 ms pulsar is possible only because the observation was made in "WSZ" mode, which tags each photon with the full 0.5 ms time resolution of the the spacecraft clock. Although the spacecraft clock drifts at an average rate of $\sim 1 \times 10^{-8}$, the times in the data stream are kept to within ± 0.3 ms of UTC by the following procedure. Each time the clock drifts to +0.3 ms, a jump of –0.6 ms is applied to the data. This correction is applied on average 3.2 times per day. During the

span of our observation, 61 such corrections were applied. By interpolating between these known discontinuities, we reduced this particular source of error to $\sim$ 0.1 ms, resulting in a slightly sharper pulse profile. Another requirement for limiting systematic errors to 0.1 ms is knowledge of the satellite ephemeris to an accuracy of 30 km along its orbit. This condition has not been verified to our knowledge, but the design specification of 10 km is well within our requirements. Since the time resolution is still no better than 0.5 ms, fine details in the pulse profile may not be significant. In particular, the 20 bin light curve in Figure 1 oversamples the true time resolution by a factor of 2.

Even though we believe that the *relative* stability of the spacecraft clock was maintained to better than 0.5 ms over the 20 day span of the observation, the details of the pulse profile could also be affected by errors in *absolute* timing, if there are any. We do not believe that there are any such gross effects. For example, the *EUVE* data can itself be used to time the periastron passage of the pulsar, and the result agrees with the radio ephemeris to within $\pm$15 s. Any errors in absolute time that are smaller than this would have a negligible effect on our results.

In deriving the pulse profile in Figure 1, it is important that we deliberately *did not* search over a range of pulsar and binary parameters, since the radio ephemeris is extremely accurate for our purposes. Unlike the radio, the X-ray pulse does not have a strong, narrow feature that can be used to optimize the ephemeris. Such a search would simply introduce large, spurious features into the pulse profile. In summary, we believe that the light curve in Figure 1 is grossly accurate in terms of pulsed fraction and non-sinusoidal shape, but that the individual bin-to-bin variations are not reliable. In particular, it is not clear if the top of the light curve is flat, cusped, or round.

There are likely pitfalls in fitting the *EUVE* and *ROSAT* data jointly because the nature of the error bars are completely different. The DS flux constitutes a single data point with very high statistical accuracy, but potentially disastrous systematics. The *ROSAT* error bars, on the other hand, are dominated by counting statistics. Therefore, we have chosen to apply a method in which the *ROSAT* spectrum is first fitted over a generous grid of parameters, and then each of these trial spectra are folded through the DS effective are curve in order to find those models which are consistent with both instruments' data. In this way, the qualitatively different contribution of each to the errors can be seen. For the DS, the effective area curve used is that displayed in the Second *EUVE* Source Catalog.

In order to test whether or not the *EUVE* flux of PSR J0437–4715 is consistent with the power-law fit to the *ROSAT* spectrum, we folded each of the trial *ROSAT* spectra corresponding to the fixed grid of Figure 2 through the effective area curve of the DS. The normalization constant for each trial was individually calculated from the total *ROSAT* counts. In this way, a grid of predicted DS counts was derived for comparison with the observed number. The range of spectral parameters acceptable to the DS is approximated by assigning a $\pm$15% uncertainty to the predicted DS count rate to account for any relative errors in normalization between the effective areas of the two instruments. The resulting band of spectral parameters allowed by the DS overlaps the *ROSAT* confidence contour in Figure 2, implying that a single power law fits both instruments.

The principal contribution of the *EUVE* point is to restrict $N_{\rm H}$ to the lower end of the *ROSAT* range, namely $(5-8) \times 10^{19}$ cm^{-2}. This is consistent with what we know about the total column density in this direction from the adjacent Seyfert galaxy, which

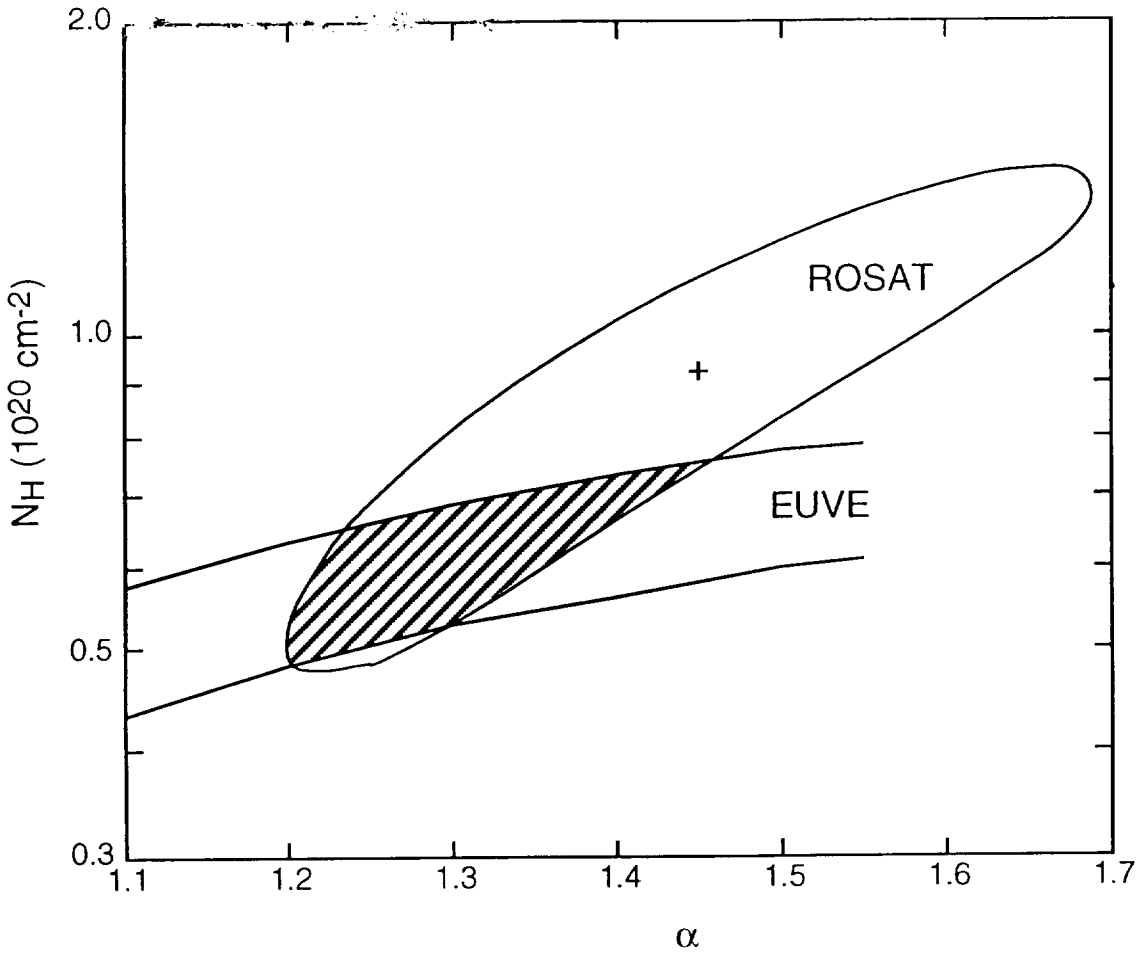

FIG. 2.– Confidence contours for the power-law fit. The 90% confidence level for the *ROSAT* PSPC spectrum corresponds to the case of two interesting parameters $(\alpha, N_{\rm H})$. The *EUVE* contour corresponds to agreement of the observed count rate in the DS to within $\pm 15\%$ of the value predicted by folding the corresponding *ROSAT* spectrum through the DS effective area curve. The shaded region indicates the spectral range jointly allowed by both instruments.

has $N_{\rm H} = (1.01 \pm 0.16) \times 10^{20}$ cm^{-2}, and with the dispersion measure that indicates an ionized column of $N_{\rm e} \sim 8 \times 10^{18}$ cm^{-2} toward the pulsar. At a Galactic latitude of $-42°$, the 140 pc line of sight to the pulsar passes through a neutral gas column about half that to infinity. Thus, the measured range of $(5 - 8) \times 10^{19}$ cm^{-2} is within expected limits.

Our result contradicts the claim of Edelstein *et al.* (1995) that their earlier *EUVE* observation is inconsistent with a power-law fit to the *ROSAT* data unless the column density is as high as 2.5×10^{20} cm^{-2}, an unacceptably large value. We speculate that they disregarded the *range* of individual normalizations that would be associated with a grid of acceptable fits. Our own power-law folds though both instruments are consistent with $N_{\rm H} = (5 - 8) \times 10^{19}$ cm^{-2}.

Given the acceptable fit of a single power law with reasonable column density to both the *EUVE* and *ROSAT* data, and the lack of evidence for a blackbody component, one would be tempted to call a halt to the spectral fitting at this point. In fact, the $\chi^2_{\rm min}$ of the power-law model is almost *too* small. The probability of χ^2 exceeding the observed value of 19.6 is 77%. Therefore, the statistical quality of the data may not be good enough to support tests for deviations from a power law. Nevertheless, there are weak observational reasons, and strong theoretical reasons, to examine what contribution a blackbody component *might* make to the soft X-ray flux without violating observed limits. The observational reasons are the possible variation in pulsed fraction as a function of energy, and the fact that the peaks are not so strong and sharp as to rule out a contribution of a hot surface to either the pulsed or the unpulsed flux. The theoretical reason has do with estimates of polar cap heating from the impact of particles accelerated in the pulsar magnetosphere that predict thermal luminosities which are not insignificant compared to the observed X-ray luminosity of PSR J0437–4715. That some younger pulsars seem to display such components is also a motivation to examine such a scenario. Accordingly, we analyzed two-component models, the one illustrated here involving a power law plus blackbody.

The model spectrum takes the form

$$F(E) = C\left(\frac{E^3}{e^{E/kT}-1} + f\,E^{-\alpha}\right) e^{-\sigma(E)N_{\rm H}} \quad {\rm keV\,cm^{-2}\,s^{-1}\,keV^{-1}}. \tag{1}$$

The method that we use in exploring the parameter space of this model is as follows. A full four-dimensional χ^2 grid is searched for acceptable values of the temperature T, energy spectral index α, column density $N_{\rm H}$, and power-law fraction f. For each trial spectrum, the overall normalization constant C is that which matches the total counts. Confidence limits can then be found by projecting the χ^2 grid onto any lower dimensional surface of interest.

The 90% confidence contour for the blackbody component in the $(T, N_{\rm H})$ plane is shown in Figure 3. The decrease in $\chi^2_{\rm min}$ from 19.6 (in the power-law fit) to 12.8 justifies the addition of two parameters at the 99% level, according to the F test. However, this $\chi^2_{\rm min}$ is probably *too* small, as discussed above. The probability of χ^2 exceeding 12.8 is 95.6%. A column density less than 10^{19} cm^{-2} is formally possible in this model because the blackbody has an intrinsic downturn at low energy. Such a low value is conceivable if most of the interstellar medium in the line of sight is in the hot phase, a possibility which is not contradicted by any measurement that we are aware of.

If we adopt the dispersion-measure distance of 140 pc, then each trial fit can be translated to a surface area for the blackbody component. Because the fitted temperatures are relatively large, $T = (1.0-3.3)\times10^6$ K, the corresponding surface areas are quite small. The radius of the inferred hot spot ranges from 50–600 m, as indicated by the dashed contours in Figure 3, and its bolometric luminosity is $\sim 8.4\times10^{29}$ ergs s^{-1}. In comparison, the standard radius of the open field-line polar cap, $r_{\rm p} = (R\Omega/c)^{1/2}R$, is 1.9 km. Note that these area estimates are uncertain by a factor of a few because of the time-averaged projection effects that depend on the unknown viewing geometry of the assumed small, hot region. We also neglect the possible deviations of realistic model atmospheres from a

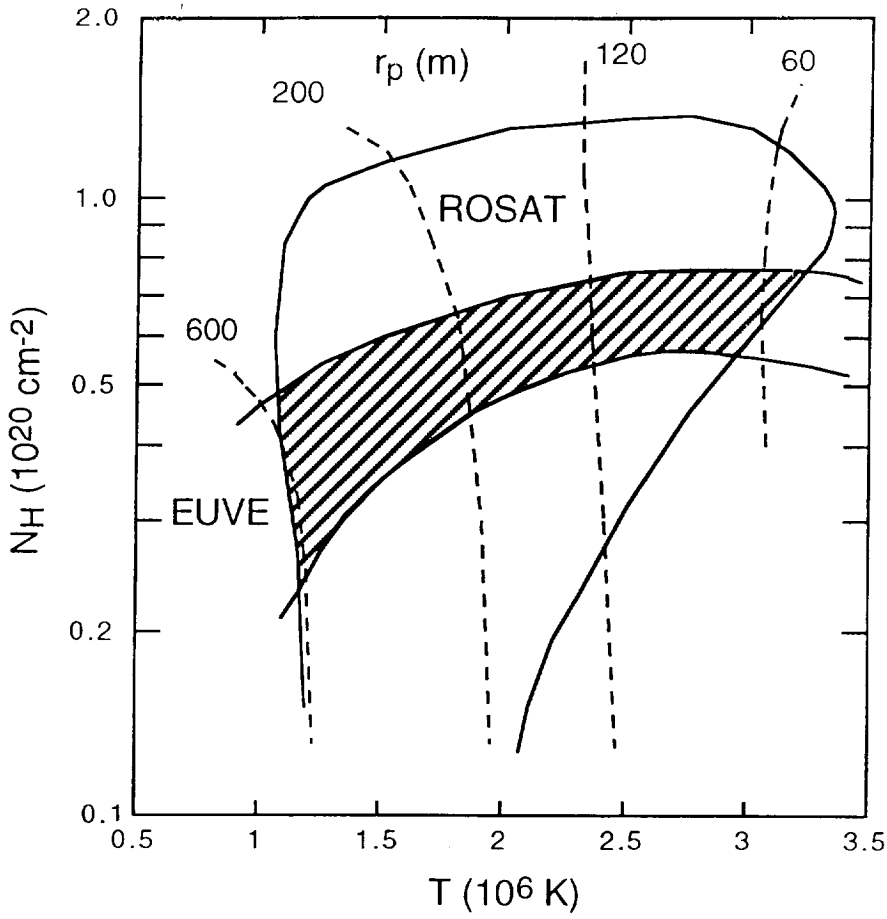

FIG. 3.– Confidence contours for the parameters of the blackbody X-ray component in the power law plus blackbody fit. The 90% confidence level for the *ROSAT* PSPC spectrum corresponds to the case of three interesting parameters ($T, N_{\rm H}, C$). The contour marked *EUVE* corresponds to agreement of the observed count rate in the DS to within $\pm 15\%$ of the value predicted by folding the corresponding *ROSAT* spectrum through the DS effective area curve. The shaded region indicates the spectral range jointly allowed by both instruments. The dashed lines are the corresponding radii, in meters, of the emitting area at the assumed distance of 140 pc.

blackbody, which tend to lower the temperatures and increase the surface area that can fit a given observed spectrum. In view of the weak need for a thermal component to begin with, the areas could be interpreted as upper limits rather than estimates.

Finally, we superpose a contour that corresponds to agreement with the observed *EUVE* DS flux. As before, the main contribution of the DS measurement is to restrict the column density to less than 8×10^{19} cm^{-2}. It is important to realize that, in this model, it is still the power law that makes the dominant contribution to the *EUVE* detection. The thermal component contributes less than 10% of the flux below 0.2 keV. At 0.7 keV, however, the thermal contribution is about 40% of the total, which could be consistent with the slight increase in pulsed fraction at that energy (47% as opposed to $\sim$ 32% on

average). This scenario would require the thermal component to be more highly pulsed than the power law, and nevertheless have the same phase.

Possible interpretations of the pulse profile include hot spots at the magnetic polar caps, and beaming of nonthermal radiation along the open magnetic field lines. Quite specific information about the magnetic geometry and viewing direction of pulsars can be derived from the rotating vector model of the radio polarization, which often represents the sweep of position angle with phase very well. In the case of PSR J0437-4715, there is significant radio emission over at least 80% of the pulse period, but the complex details of the position angle variations are not fitted well by the simple model. Deviations are not unexpected from millisecond pulsars, since the emission region is likely to be close enough to the surface for higher order multipoles of the magnetic field to have a significant effect on the polarization. Although the pulse profile is itself complex, Manchester & Johnston (1995) concluded that the strong "core" component indicates that the magnetic axis crosses close to our line of sight. Despite possible complicating details, they conclude that the overall shape of the position angle variation favors magnetic inclination angle $\alpha = 145°$, and viewing angle $\zeta = 140°$, both measured from the rotation axis. In this geometry, and for a dipole centered on the star, the opposite magnetic pole remains more than 15° below the limb at all times, which is consistent with the absence of an interpulse in the radio, and in the X-ray if the latter is at least moderately beamed.

This geometry does not clearly distinguish between thermal and nonthermal models for the X-ray pulse for two reasons. First, thermal emission from the opposite polar cap may still be visible because of strong light bending at the surface of the neutron star. Indeed, such an effect may be responsible for some of the substantial X-ray emission seen at pulse minimum. Detailed modelling of the light bending effect in this specific geometry for various assumed values of M/R would be necessary to determine whether the observed pulse profile is consistent with thermal emission from both poles. Second, the simple centered dipole may not be a correct description of the *surface* magnetic field geometry, even to a first approximation. Indeed, there are theoretical reasons to think that this is the case for millisecond pulsars, and observations of thermal X-ray components in ordinary pulsars always show only one pulse per rotation period. As mentioned earlier, the coincidence of the X-ray phase at all energies is problematic for models in which both thermal and nonthermal processes contribute. Time of flight delays and differential relativistic aberration between the pulsar's surface and magnetosphere are substantial. Ultimately, the absolute time of arrival of the X-ray pulse with respect to the radio will reveal important information about the relative heights of the radio and X-ray emitting regions, but this analysis is not yet reliable at the ms level. For these reasons, we must rely on the X-ray spectrum for additional clues about the sources of emission.

If most of the soft X-ray emission from PSR J0437–4715 is to be described as a nonthermal power law, then it must flatten in the far ultraviolet so as not to exceed the observed brightness of the $B = 22$ optical companion. The X-ray power law of slope 1.45 would extrapolate to $B = 16.7$. A power law connecting the actual blue flux to the observed X-ray flux at 200 eV would have a spectral index of 0.30. The real ultraviolet spectrum must therefore be flatter on average than 0.3. The X-ray and assumed far UV spectrum could be synchrotron radiation in the $< 3.4 \times 10^8$ G magnetic field near the surface of the neutron star, as the cyclotron frequency eB/mc falls in the visible band. Electrons

with Lorentz factor $\gamma > 10$ would produce the soft X-rays that we see. Alternatively, synchrotron emission from the outer magnetosphere, within the light cylinder of radius $r_{\rm lc} = 2.7 \times 10^7$ cm, could involve electrons of $\gamma > 2000$ and $B \sim 10^4$ G. Our default interpretation is that most of the X-ray flux from PSR J0437–4715 is magnetospheric in origin, similar to that of ordinary, young pulsars, with the rather low pulsed fraction perhaps resulting from a broader beaming pattern related to the large opening angle of the open field-line region expected for millisecond pulsars, and observed in the radio.

The two-component models investigated here favor blackbody emission at temperatures of either $(4 - 12) \times 10^5$ K, or $(1.0 - 3.3) \times 10^6$ K, and from areas that are much smaller than the full surface of the neutron star. If these are taken as detections rather than upper limits, it would mean that thermal reheating is taking place, as neutron stars in all standard calculations cool below 10^5 K after 10^6 yr. The observation that the thermally emitting region may be comparable to or smaller than the open field-line polar cap, of radius $r_{\rm p} = 1.9$ km, motivates us to consider surface reheating by the bombardment of the polar cap region by energetic particles produced in the accelerators that are responsible for radio and high-energy emission. Direct evidence for such a process is seen in the X-ray emission from Geminga and other intermediate-age pulsars, and especially from PSR B1929+10, a 3×10^6 yr old pulsar in which the 3×10^6 K blackbody emission comes from an area less than 50 m in radius. The same mechanism may also explain the weak X-ray flux from the 1.7×10^7 yr old pulsar PSR B0950+08.

The maximum efficiency of heating by magnetospheric processes can be estimated by multiplying the Goldreich-Julian current density by the area of the polar caps to find an upper limit on the impacting particle flux,

$$\dot{N} < 2 \left(\frac{\Omega B}{2\pi e} \right) \left(\frac{\pi}{2} \frac{R\Omega}{c} \right) R^2 = 1.4 \times 10^{31} \ {\rm s}^{-1}. \tag{2}$$

The residual energy with which those particles impact the polar cap after radiating most of their energy via curvature radiation is,

$$E = \left[\frac{2e^2 \, \Omega}{mc^3} \ln \left(\frac{r_{\rm in}}{R} \right) \right]^{-1/3} mc^2 \sim 2.3 \ {\rm ergs}, \tag{3}$$

Here, $r_{\rm in}$ is the inner radius of the accelerator region, which we take to be $\sim 10^7$ cm in this case. The maximum power brought down to the polar cap is then $L_{\rm p} = \dot{N} E \leq 3.2 \times 10^{31}$ ergs s^{-1}.

This maximum heating rate is undoubtedly not operating because, if it were, the same accelerated particles would be radiating nearly the full spin-down power of PSR J0437–4715 in high-energy γ-rays. Rather, we suppose that the upper limit $L_\gamma < 1.7 \times 10^{32} = 0.04 \, I \Omega \dot{\Omega}$ implies that either the size or the efficiency of the accelerator is less than 0.04 times the maximum value. Scaling the surface heating rate accordingly yields $L_{\rm p} < 1.3 \times 10^{30}$ ergs s^{-1}. This is a comfortable value, for it can accommodate an interpretation of part of the observed X-ray luminosity as thermal without violating any of the upper limits. We conclude that even though the evidence for a thermal component is weak, a fraction of the observed X-ray luminosity could be understood as arising from the polar caps heated by

particles accelerated in the magnetosphere without violating observational limits on γ-ray emission.

The main purpose of this investigation was to examine the origin of the soft X-ray flux in the 5.75 ms pulsar J0437–4715. Plausible alternatives include magnetospheric synchrotron emission, surface thermal emission, and, for the unpulsed flux only, synchrotron emission at the pulsar wind's bow shock. Unfortunately, it is still not possible to rule out significant contributions from any of these mechanisms, as the light curve and spectrum do not strongly discriminate among them. The light curve in the *EUVE* DS (65–120 Å) consists of a single broad pulse containing $\sim 27\%$ of the flux, similar to that of the *ROSAT* data in the overlapping energy band. A combined analysis of the *EUVE* and *ROSAT* data is consistent with a power-law spectrum of intrinsic luminosity 5×10^{30} ergs s^{-1} in the 0.1–2.4 keV band, and $\alpha = 1.2 - 1.5$. The effect of the *EUVE* flux is to limit the column density $N_{\rm H}$ to the range $(5 - 8) \times 10^{19}$ cm^{-2}. For comparison, a nearby soft X-ray Seyfert galaxy determines the total Galactic column in this direction, $N_{\rm H} = 1 \times 10^{20}$ cm^{-2}.

When we apply two-component spectral fits to the combined *EUVE/ROSAT* data, we find that a small, hot polar cap of radius $50 - 600$ m and temperature $(1.0 - 3.3) \times 10^6$ K could also be present. The principal motivation for including this component is a possible increase at $\sim$ 0.9 keV in the pulsed fraction as a function of energy. The luminosity of such a region, $\sim 8 \times 10^{29}$ ergs s^{-1}, would most likely be powered by the impact of high-energy particles accelerated in the magnetosphere and flowing down along the open field lines. Alternatively, a larger region with $T_1 = (4 - 12) \times 10^5$ K and $A_1 < 200$ km^2, might contribute the majority of the *EUVE* and soft X-ray flux, but only if a smaller, hotter component were present as well. Purely thermal models permit values of $N_{\rm H}$ as low as 10^{19} cm^{-2}. Scenarios in which both surface thermal emission and magnetospheric processes contribute must face the question of why the pulse phase is the same at all X-ray energies.

We are not confident that the existence of a small, thermally emitting region will stand up to detailed modelling which takes into account the magnetic and viewing geometry inferred from the sweep of radio polarization angle. Whereas the modulation due to the thermal component would have to be very large to cause an observable energy dependence, the actual modulation from a polar cap may be small because it remains more than 15° above the limb at all times, according to the results of the rotating vector model. This, plus the additional flux bent around the horizon from the opposite polar cap, may conspire to keep the pulsed fraction small. Of course, this potential difficulty could be sidestepped by abandoning the assumption of a simple centered dipole, and assigning the polar caps to arbitrary locations on the star.

2. A Long EUVE Observation of the Seyfert Galaxy RX J0437.4–4711

The Seyfert galaxy RX J0437.4–4711 was discovered in the *ROSAT* All-Sky Survey and then targeted for a pointed *ROSAT* observation. In the same *ROSAT* field, the binary millisecond pulsar PSR J0437–4715 was detected serendipitously only 4′.2 from the Seyfert. Subsequently, we performed a long observation of both objects with the *Extreme Ultraviolet Explorer* satellite (*EUVE*). In a separate paper about the pulsar, we commented briefly upon the Seyfert galaxy, and used its X-ray spectrum to obtain an upper limit on the interstellar medium column density to the pulsar. We also noted that the Seyfert galaxy should be identified with EUVE J0437–471 as listed in the Second *EUVE* Source Catalog, and with the *Einstein* Slew Survey source 1ES 0435–472, whose position is consistent with that of the *ROSAT* source. The J2000 optical position of the Seyfert galaxy is $4^{\rm h}37^{\rm m}28^{\rm s}.0$; $-47°11'27''$. A visible spectrum obtained by J. Schachter shows that it is an ordinary Seyfert 1 galaxy at $z = 0.052$. There is, apparently, no other information in the literature on this object.

The field of RX J0437.4–4711 was observed by *EUVE* during a 20 day period between 1994 October 23 and November 12, during which a valid exposure time of 495,897 s was obtained in the Deep Survey (DS) instrument during nighttime passes. Events occurring when the line of sight to the source passed less than 450 km above the Earth's limb were rejected in this analysis. A total of 26,326 counts were collected from the Seyfert through the Lexan filter, as determined in a 63″ radius extraction aperture. Background subtraction yielded an estimated 24,262 net counts from the source. After accounting for deadtime and "Primbsching" (loss of counts due to telemetry sharing), the effective exposure time is reduced to 449,034 s. The corrected mean count rate is thus 0.0540 s^{-1}.

The DS light curve corrected for dead time and Primbsching is shown in Figure 4. Each point represents one spacecraft orbit, with an average 27 minutes each of nighttime data. The light curve thus comprises 308 points uniformly sampled with a period of 95 minutes, although the individual exposure times vary considerably because of the varying effects of the South Atlantic Anomaly (SAA). Since the background counts are less than 10% of the source on average, the error bars are dominated by counting statistics of the source itself, and not by background or systematic effects.

Large-amplitude variability by a factor of 4 over the 20 day period is evident in the light curve. The most rapid changes are characterized by a minimum doubling time of 5 hr, and are frequent during the second half of the observation when the source is in its highest, flaring state. In contrast, the variability during the first half of the observation is slower, and the average intensity is lower. These features are also seen in the power spectrum, discussed in the next section. Most notably, the rapid flares seem to have a period of 0.9 days.

The 20 day *EUVE* observation of RX J0437.4–4711 constitutes a uniformly sampled soft X-ray light curve of a highly variable Seyfert galaxy whose power spectrum can be examined on timescales from 3 hr to several days. This is the range of timescales in which one might hope to find periods or quasi-periodic oscillations (QPOs) corresponding to orbital motion in the inner accretion disk around black holes of mass $10^7 - 10^9\,M_\odot$. Figure 5a shows the power spectrum of the entire DS light curve. There is considerable power at low frequencies, corresponding to the large-amplitude modulation in the light

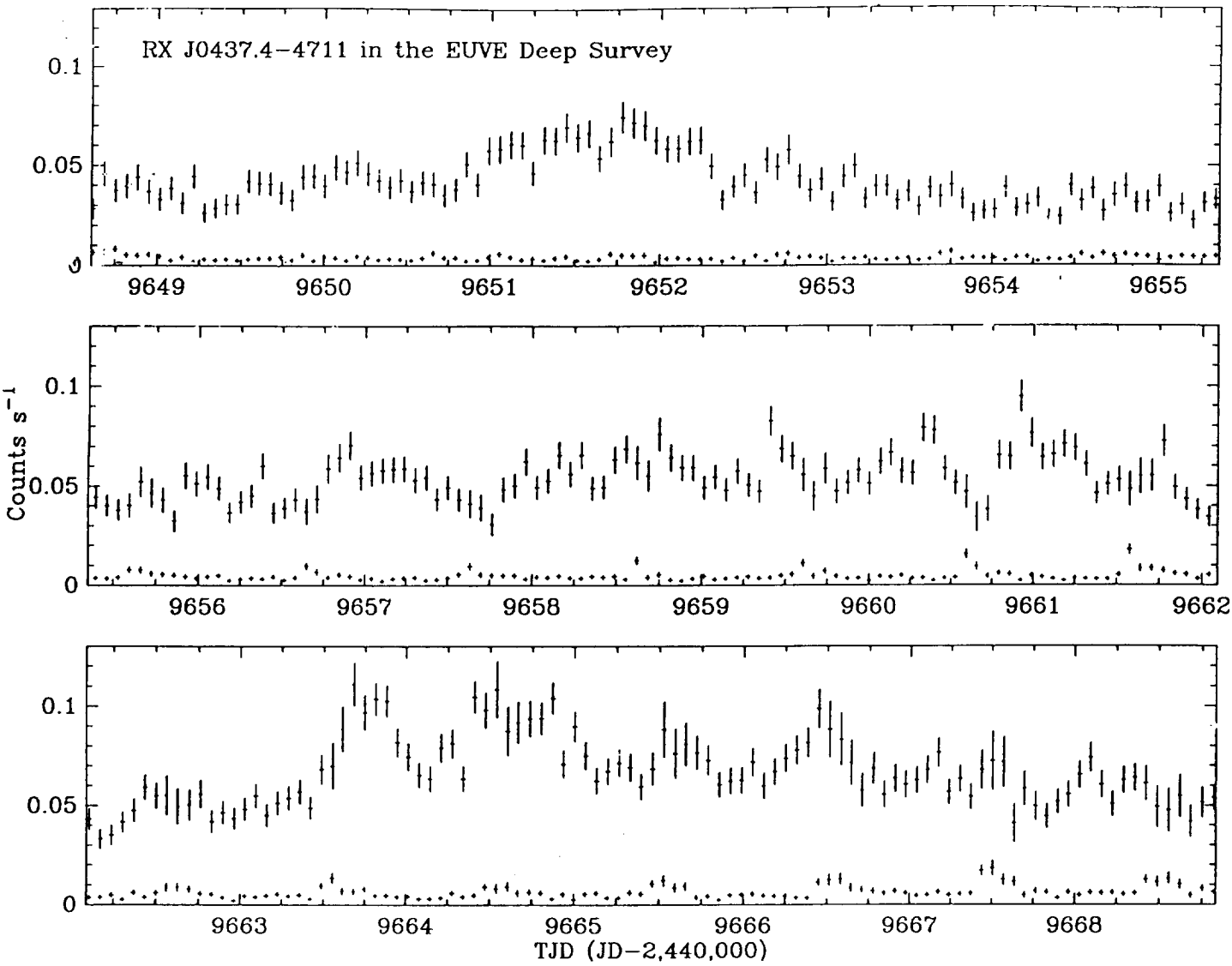

FIG. 4.– Light curve of RX J0437.4–4711 in the *EUVE* Deep Survey imager, after correction for dead time and "Primbsching." The observation began on TJD 9648.601, corresponding to 1994 October 23, 2:26 UTC. Each point corresponds to one satellite orbit. The small points along the bottom represent the background level in the same size aperture as the source.

curve on timescales of 4 days and longer. We also constructed a logarithmically binned and averaged power spectrum in Figure 5b in order to estimate its continuum slope. Although very noisy, its slope is consistent with a value of -1.25 ± 0.25 in the interval $10^{-6.0}$ to $10^{-4.1}$ Hz, where the limits correspond to half the length of the observation and the Nyquist frequency, respectively. An additional interpretation of Figure 5b is that any

break in the slope of the power spectrum in this frequency range is probably not greater than 0.5.

Figure 5a also shows that there is a possible signal at a period of 0.906 ± 0.018 days, which is well separated from the low-frequency noise. The structure that is responsible for this signal is evident in the light curve of Figure 4. In Figure 6, we graph the light curve folded at a period of 0.906 days, after removing the slower variations by fitting with a fourth-order polynomial. Only the second half of the observation, beginning on TJD 9659 when the source enters its more active phase, is included in the folded light curve of Figure 6. The amplitude of modulation is $\pm 12\%$.

We have looked for systematic effects that might be expected to contaminate the power spectrum with a signal at this period, but we have not found any. Most notably, there is no signal at a period of 0.982 days that might have been generated by passages through the SAA, even though there is a very strong modulation in the dead-time correction factor at this period. The observed signal at 0.906 days is well separated from the 0.982 day period of the SAA passages, and cannot be identified with it. We cannot identify any other instrumental or terrestrial effects that could be responsible for power at 0.906 d.

It is difficult to assign a statistical significance to this periodic feature, since it is superposed on a continuum of power which is itself poorly characterized. Furthermore, the signal is not clearly present throughout the entire 20 day observation. Therefore, there is no strong reason to believe that it is a *persistent* feature of the light curve. Although theory may accommodate or even favor *transient* periods in Seyfert galaxies, the observational proof of the existence of such a phenomenon is obviously more challenging than the demonstration of a true period. In view of these difficulties, we do not regard these data as a strong demonstration of the periodic nature of the source.

In addition to the light curve obtained by the DS, the *EUVE* short-wavelength spectrometer provides a high-resolution spectral detection of RX J0437.4–4711 in the 70–110 Å range that can be examined for emission or absorption features. Only two other Seyfert galaxies, Mrk 478 and NGC 5548, have been reported to be detected in this instrument.

In order to optimize the signal-to-noise ratio of the extracted spectrum, we used only the times when the source count rate was > 0.06 s^{-1} *and* the background was low. Although the spectral shape might be a function of intensity and/or time, we find that the *EUVE* spectrum is well fitted by the power-law parameters that best describe the *ROSAT* data, namely, $\alpha = 1.56$ and $N_{\rm H} = 1 \times 10^{20}$ cm^{-2}. There is no evidence of emission lines in the spectrum. Figure 7 shows the *EUVE* spectrum and the continuum model fitted to it. It is also seen that column densities that differ by $\pm 5 \times 10^{19}$ cm^{-2} from the best value can probably be rejected. The shape of the spectrum is not very sensitive to the assumed power-law index, and cannot be used to test for deviation from the value determined by *ROSAT*.

A unique aspect of the *EUVE* observation of RX J0437.4–4711 is its long light curve which we have used to measure the power spectrum of soft X-ray variability at low frequencies. Such long X-ray observations of active galactic nuclei are rare. Although several comparably long X-ray light curves of quasars near the ecliptic poles were obtained by the *ROSAT* All-Sky Survey, those particular objects did not happen to vary during the monitoring period. The more recent reverberation-mapping campaigns have been longer in duration, but they are not sensitive to X-ray variability on timescales of hours to a

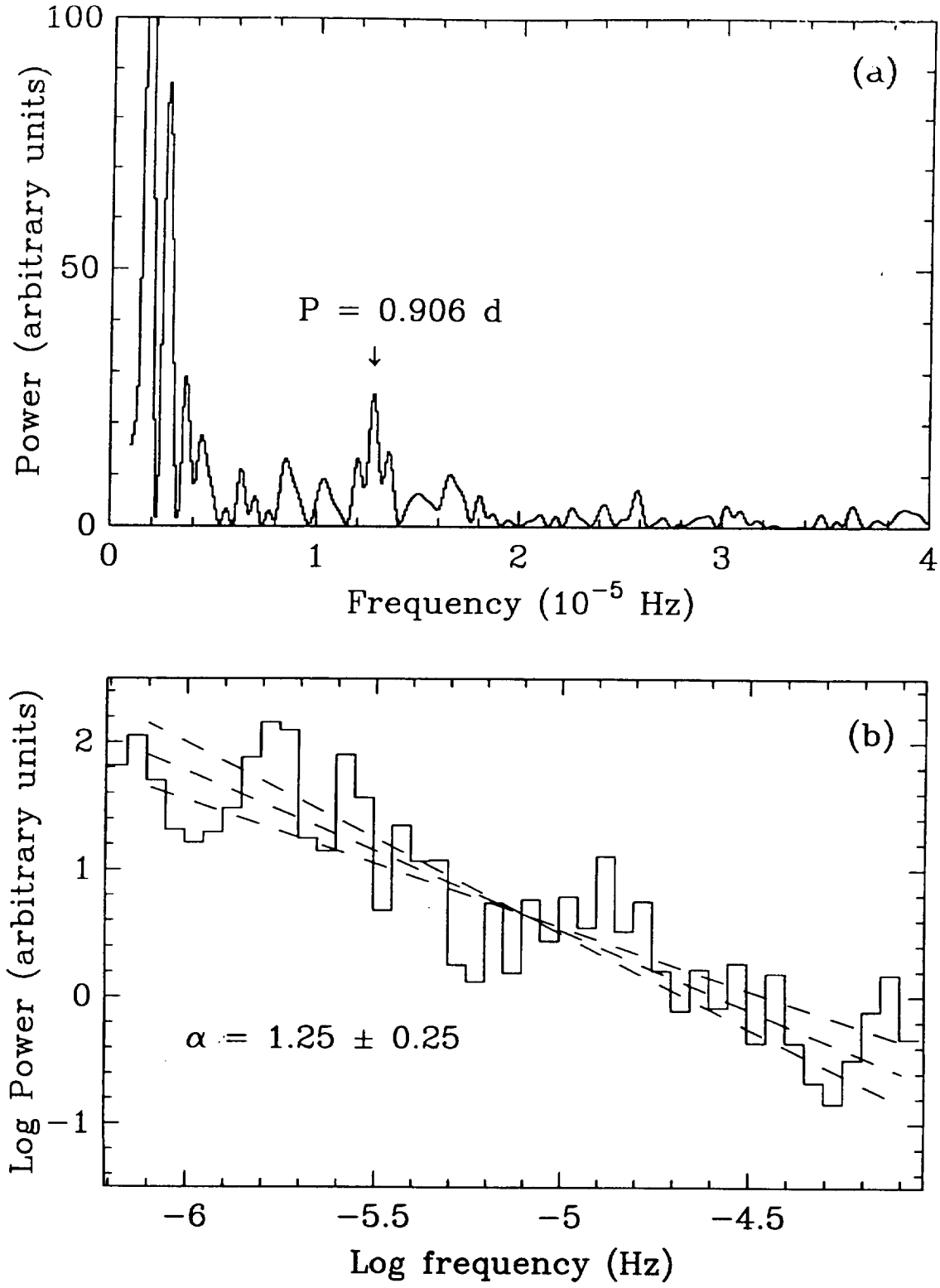

FIG. 5.– (a) Power spectrum of the *EUVE* DS light curve. A possible signal at 0.906 days is marked. (b) The power spectrum logarithmically binned and fitted to a power law of slope -1.25 ± 0.25, as indicated by the dashed lines.

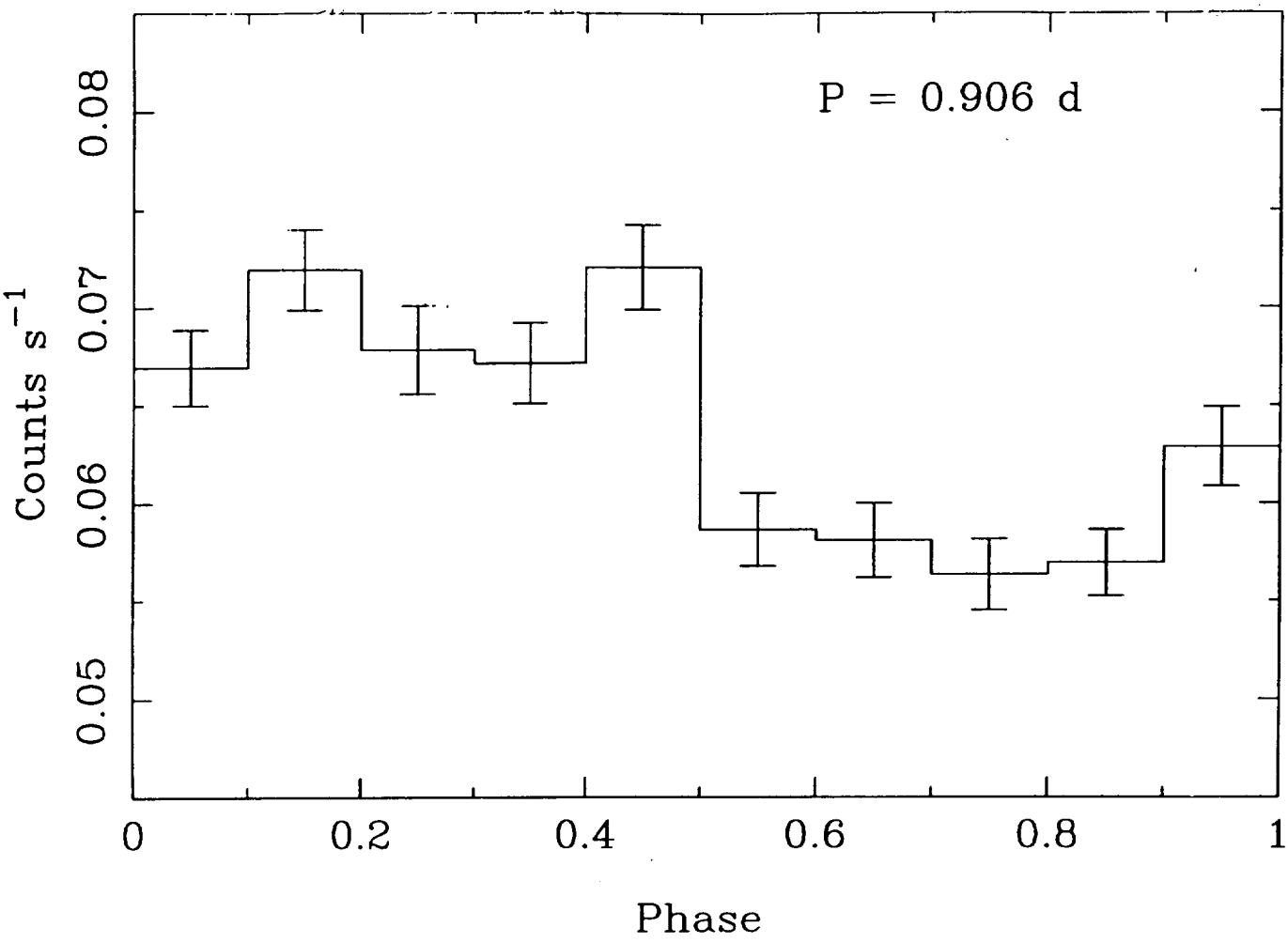

FIG. 6.– DS light curve folded at the 0.906 day period, after detrending with a fourth-order polynomial. Only data after TJD 9659.0 (phase 0) are included.

few days. The *EXOSAT* long-look observations of Seyfert galaxies provided continuous light curves with higher count rates than *EUVE*, but the longest was 3 days in length so did not sample variability on timesscales longer than 1.5 days. There have been several analyses of possible QPO features with periods of 1 hr or less in the *EXOSAT* observations of NGC 4051 and NGC 5548.

The power spectrum at low frequencies can distinguish between shot-noise and rotating spot (accretion disk) models. The latter predicts periodic or quasi-periodic behavior, not unlike the possible signal we see at 0.9 days, although it should be noted that the width of the 0.9 day feature in Figure 5a is not significantly resolved into a QPO. The shot-noise model, on the other hand, predicts that there will be two breaks in the power spectrum, corresponding to the shots with the shortest and longest decay times. If there are such breaks, they have not yet been seen clearly at either low or high frequencies. However, *EXOSAT* was able to measure the shape of the power spectrum accurately only between about $10^{-4.5}$ and $10^{-3.5}$ Hz. Our own data, which might have revealed a low-frequency

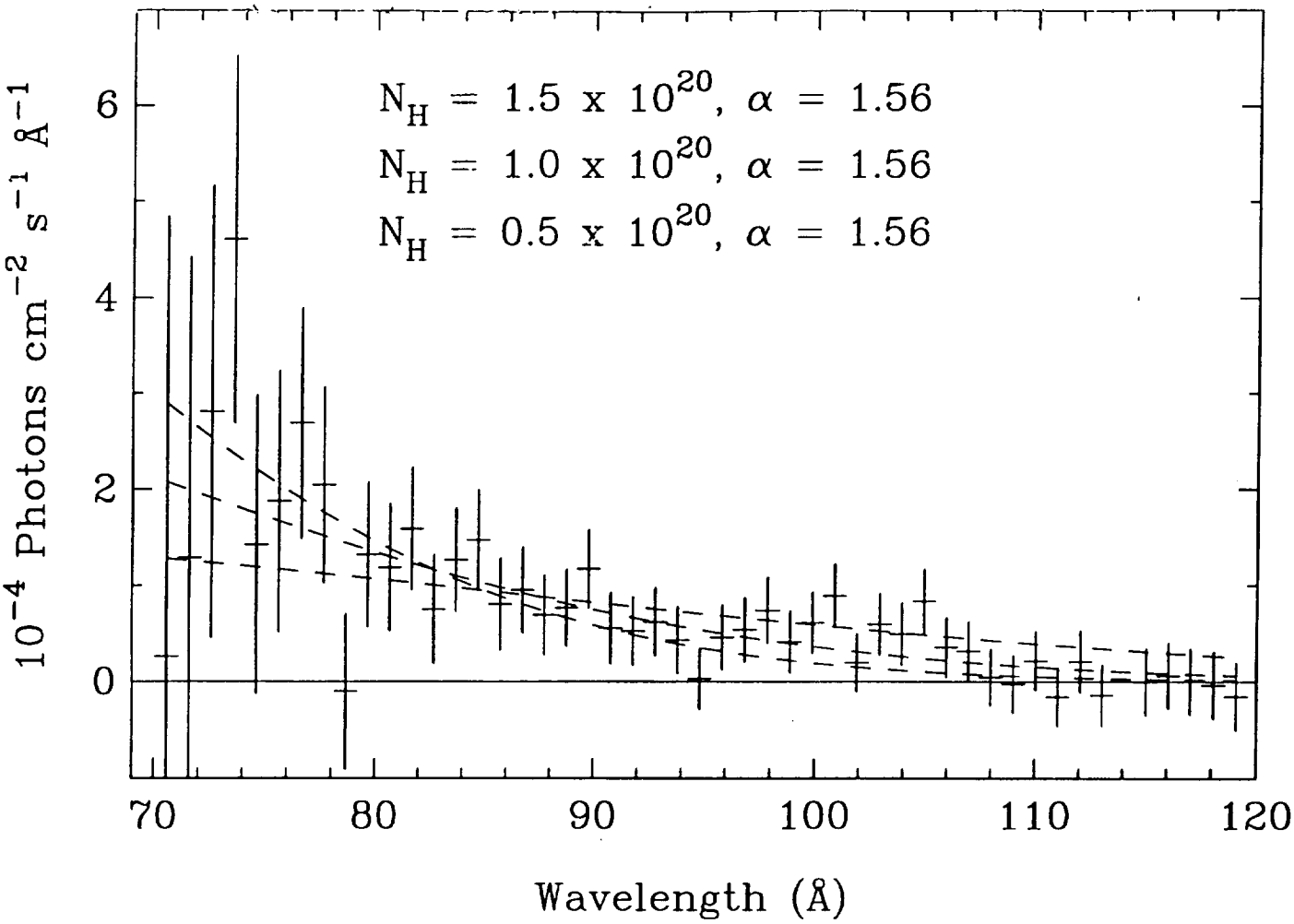

FIG. 7. - Spectrum extracted from the *EUVE* short-wavelength spectrometer. The fitted models correspond to a power law of energy index 1.56 as found by the *ROSAT* PSPC, but with varying values of intervening column density N_H.

break below 10^{-5} Hz, cannot be claimed to have done so. Instead, the slope of -1.25 ± 0.25 that we measure between $10^{-6.0}$ and $10^{-4.1}$ Hz is consistent with the slopes measured by *EXOSAT* for other Seyfert galaxies. The divergence of the power at low frequencies, at least in RX J0437.4–4711, continues down to a time scale of at least 10 days. Neither do we know if we should expect a break above 10^{-4} Hz. Some of the *EXOSAT* power spectra, most notably that of NGC 5506, have slopes of –2, but some do not.

It is particularly important to measure variability in the EUV because of the possibility that this component contains the bulk of the emission from the inner accretion disk. Therefore, even longer observations in the EUV will be needed to reveal the characteristic timescale and amplitude of variability at the peak of the Seyfert spectral energy distribution.

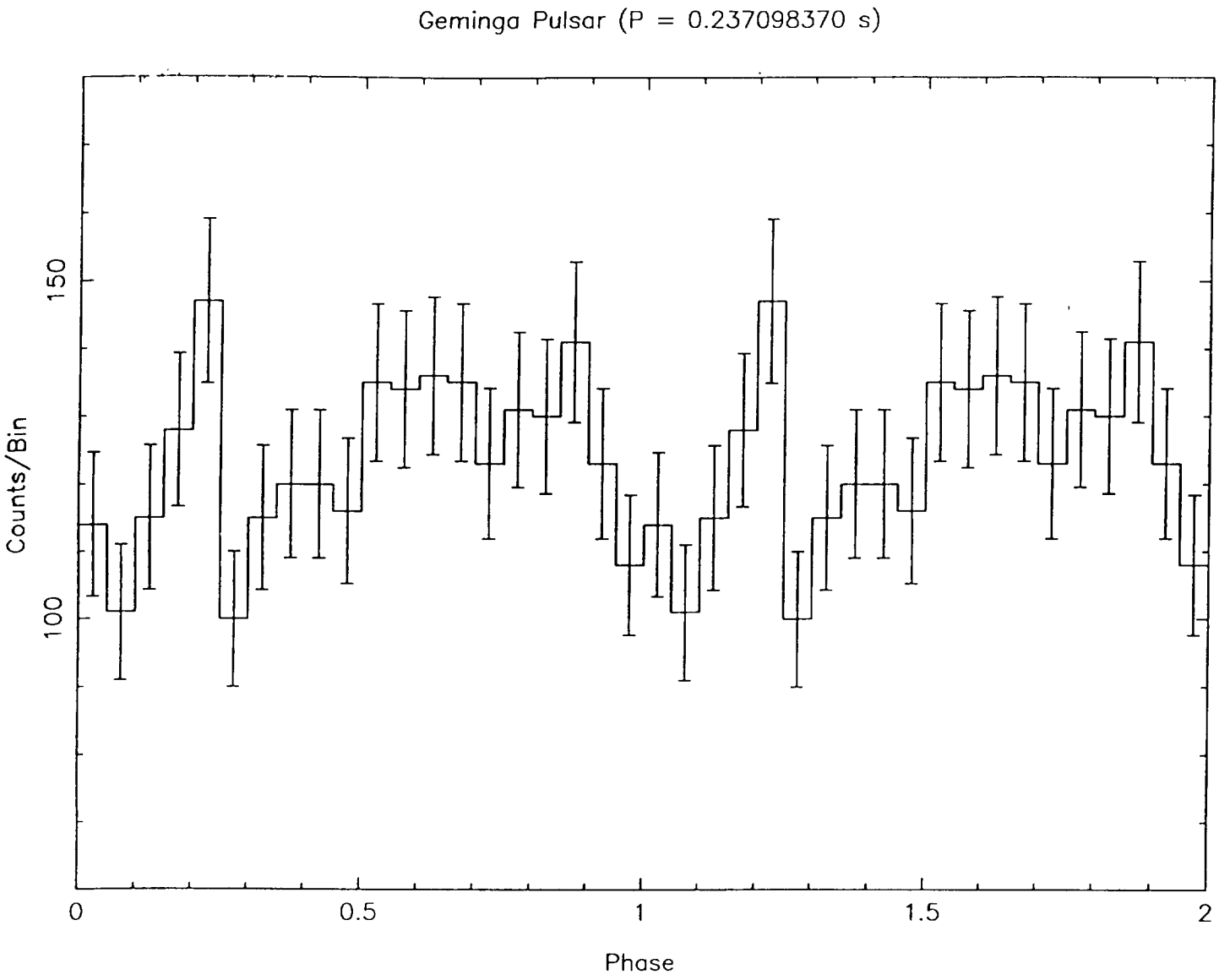

FIG. 8.– Pulse profile of the Geminga pulsar from the *EUVE* Deep Survey instrument. Background has not been subtracted. The phase is arbitrary. The data are repeated for two cycles to guide the eye.

3. EUVE Observation of the Geminga Pulsar

The Geminga pulsar was observed by *EUVE* for 251,000 s in 1994 January. Approximately 2100 counts were detected in the Deep Survey instrument. The data were reduced in the same manner as described in §1 for PSR J0437–4715. The resulting pulse profile, folded at the 0.237 s period, is shown in Figure 8. It resembles the soft X-ray pulse profile obtained by *ROSAT* in the overlapping energy band, although the *EUVE* flux is about 50% lower for the range of spectral parameters that fit the *ROSAT* data. I am presently investigating the possible reasons for this discrepancy. Geminga presents an unusually difficult problem because its multicomponent X-ray spectrum and pulse profile are indicative of a complex distribution of surface emission, and possibly a contribution

from nonthermal emission as well. These are impossible to disentangle in the *EUVE* data by itself. Therefore, I will do a joint analysis of the *EUVE*, *ROSAT*, and *ASCA* data, all of which detect Geminga and its pulsations. Various multicomponent model spectra will be fitted to determine whether the hard X-ray component is thermal or nonthermal. Pulse profiles in different energy bands will be compared, and phase-resolved spectroscopy will be done.

I have also begun a collaboration with George Pavlov of Penn State University and his group of collaborators at the Ioffe Institute of Physics and Technology in St. Petersburg. This group calculates model atmospheres of neutron stars taking into account the extreme properties of atoms in strong magnetic fields, and the highly anisotropic radiative transfer that occurs in such fields. We will apply these models first to the spectra and pulse profiles of Geminga and PSR J0437–4715 that are already in hand, as examples of a strong field and a weak field neutron star. It is important to use realistic model atmospheres in interpreting the X-ray data, since these models completely change what one infers for the temperature and the size of the surface X-ray emitting region. Even in a case of known magnetic and viewing geometries, it is necessary to employ model atmospheres to calculate the expected X-ray emission as a function of viewing angle, because the emission is highly anisotropic.

APPENDIX

Papers Published Under NASA Grant NAG 5–2569

"Soft X-ray Properties of the Binary Millisecond Pulsar PSR J0437–4715," Halpern, J. P., Martin, M., & Marshall, H. L. 1996, *Ap. J.*, **462**, 000.

"A Long *EUVE* observation of the Seyfert galaxy RX J0437.4–4711," Halpern, J. P., & Marshall, H. L. 1996, *Ap. J.*, **464**, 000.